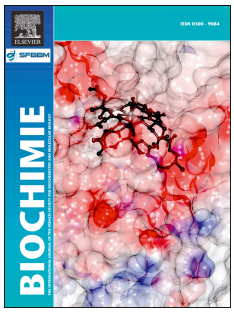

Functional and structural characterization of an endo-β-1,3-glucanase from *Euglena gracilis*

Rodrigo D. Calloni, Robertino J. Muchut, Sergio E. Garay, Diego G. Arias, Alberto A. Iglesias, Sergio A. Guerrero

PII: S0300-9084(22)00341-8

DOI: https://doi.org/10.1016/j.biochi.2022.12.016

Reference: BIOCHI 6444

To appear in: *Biochimie*

Received Date: 14 September 2022

Revised Date: 20 December 2022

Accepted Date: 23 December 2022

Please cite this article as: R.D. Calloni, R.J. Muchut, S.E. Garay, D.G. Arias, A.A. Iglesias, S.A. Guerrero, Functional and structural characterization of an endo-β-1,3-glucanase from *Euglena gracilis*, *Biochimie* (2023), doi: https://doi.org/10.1016/j.biochi.2022.12.016.

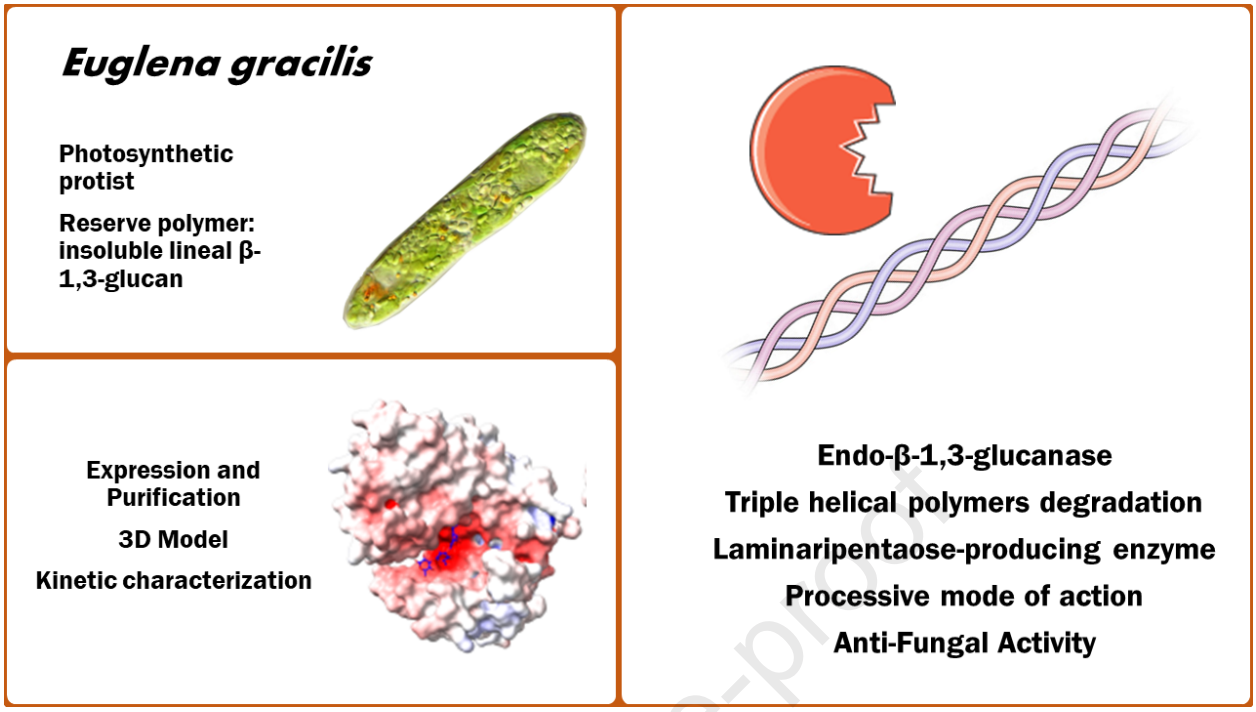

Functional and structural characterization of an endo-β-1,3-glucanase from *Euglena gracilis*

Rodrigo D. Calloni[1,2], Robertino J. Muchut[1,#], Sergio E. Garay[2], Diego G. Arias [1,2], Alberto A. Iglesias[1,2], Sergio A. Guerrero[1,2,*]

[1]Laboratorio de Enzimología Molecular. Instituto de Agrobiotecnología del Litoral (CONICET-UNL). Santa Fe. Argentina.

[2]Facultad de Bioquímica y Ciencias Biológicas. Universidad Nacional del Litoral. Santa Fe, Argentina.

[#]**Present affiliation**: CONICET and Instituto Nacional de Tecnología Agropecuaria**,** Estación Experimental Agropecuaria Reconquista, Santa Fe, Argentina.

*__Corresponding author__: Dr. Sergio A. Guerrero. Instituto de Agrobiotecnología del Litoral. (CONICET-UNL). Colectora Ruta Nacional Nº 168 km 0, Santa Fe (3000), Argentina. saguerrero@santafe-conicet.gov.ar

ABSTRACT

Endo-β-1,3-glucanases from several organisms have attracted much attention in recent years because of their capability for *in vitro* degrading β-1,3-glucan as a critical step for both biofuels production and short-chain oligosaccharides synthesis. In this study, we biochemically characterized a putative endo-β-1,3-glucanase (*Egr*GH64) belonging to the family GH64 from the single-cell protist *Euglena gracilis*. The gene coding for the enzyme was heterologously expressed in a prokaryotic expression system supplemented with 3% (v/v) ethanol to optimize the recombinant protein right folding. Thus, the produced enzyme was highly purified by immobilized-metal affinity and gel filtration chromatography. The enzymatic study demonstrated that *Egr*GH64 could hydrolyze laminarin (K_M 23.5 mg.ml^{-1},k_{cat} 1.20 s^{-1}) and also, but with less enzymatic efficiency, paramylon (K_M 20.2 mg.ml^{-1},k_{cat} 0.23 ml.mg^{-1}.s^{-1}). The major product of the hydrolysis of both substrates was laminaripentaose. The enzyme could also use ramified β-glucan from the baker's yeast cell wall as a substrate (K_M 2.10 mg.ml^{-1}, k_{cat} 0.88 ml.mg^{-1}.s^{-1}). This latter result, combined with interfacial kinetic analysis evidenced a protein's greater efficiency for the yeast polysaccharide, and a higher number of hydrolysis sites in the β-1,3/β-1,6-glucan. Concurrently, the enzyme efficiently inhibited the fungal growth when used at 1.0 mg/mL (15.4 µM). This study contributes to assigning a correct function and determining the enzymatic specificity of *Egr*GH64, which emerges as a relevant biotechnological tool for processing β-glucans.

KEYWORDS: GH64 protein; Euglenoids; paramylon; laminarin

58

1. INTRODUCTION

Euglena gracilis is a single-celled flagellate that lives in aquatic environments **[1]**. It belongs to the protist phylum Euglenozoa, incluiding kinetoplastids (bodonids and trypanosomatids), diplonemids, and symbiontids**[2–4]**. Furthermore, Euglenozoa is comprised within the Excavata group along with other parasites such as *Giardia* spp. (Fornicata) and *Trichomonas* spp. (Parabasalia),the reason for which many authors consider that the former represents the most basal eukaryotic branch **[5]**. *E. gracilis* is a microorganism capable of growing both photosynthetically (using sun light to fix atmospheric CO_2), heterotrophically (in the dark with an organic carbon source), and mixotrophically (using an organic carbon source in the light).

Whatever the growing condition, *E. gracilis* manages to accumulate different bioactive compounds inside the cell, especially paramylon and wax esters **[6,7]**, both of which are relevant due to their potential use in generating biodegradable plastics or bioethanol, in replacement of hydrocarbons. Each growth condition implies the activation of specific metabolic pathways and producing different forms of carbon accumulation. Thus, studying the biochemical, functional, and regulatory properties of the enzymes involved in the synthesis and degradation of Euglenoids reserves is important.

E. gracilis obtains the energy necessary to remain viable under anaerobic and dark conditions by degradation of paramylon, mainly linear β-1,3-polymer of glucose. An important focus of our work is to characterize enzymes involved in this protist metabolism to manage paramylon into readily fermentable glucose units. Moreover, several of the oligosaccharide products of hydrolysis exhibit various biological activities, such as anti-diabetic **[8]**,stimulating leukocytes to induce the production of cytokines **[9]**, or modulating lipid metabolism and intestinal microflora **[10]**.

Consequently, suitable endo-β-1,3-glucanases are determinants for the enzymatic preparation of well-defined glucooligosaccharides.

In *E. gracilis*, the accumulated paramylon degrades when there are energy requirements. Partial consumption of paramylon at night has been shown in autotrophic cultures **[11]**. Under anaerobic conditions, the polysaccharides is promptly degraded and converted to wax esters **[12]**. However, paramylon granules have been found as recalcitrant to enzymatic degradation, after which a consortium of different enzymes would be required for the efficient degradation of this polysaccharide **[13]**. Studies carried out through partial purifications of paramylon extracts showed the presence of enzymes with endo and exo-β-1,3-glucanase activity. **[14–16]**. Subsequently, transcriptomics studies showed a series of transcripts that code for different families of exo and endo-β-1,3-glucanases. In the endo-β-1,3- glucanases, transcripts coding for proteins that would be part of three families with this activity were identified: GH17, GH64, and GH81 **[17,18]**. Moreover, amino acid sequences of these three families were identified from paramylon-binding assay proteomics**[19]**. Recently, the simultaneous knockdown of one GH17 and two GH81 genes showed significant but partial retardation of paramylon breakdown under hypoxic conditions**[20]**. So far, only one endo-β-1,3-glucanase, belonging to the GH17 family, has been kinetically characterized**[21]**.

We identified in *E. gracilis* a transcript coding for a putative member of the GH64 family that can specifically hydrolyze glycosidic bonds in β-1,3-glucans**[17]**. In this study, the gene coding for an endo-β-1,3-glucanase (EC 3.2.1.39) in *E. gracilis* (*Egrgh64*) was expressed using a standard *Escherichia coli* expression system. Two-step procedures allowed the high purifying of the recombinant protein. The catalytic properties of *Egr*GH64 were determined, including the enzyme's ability to hydrolyze β-

glucans containing lineal (β-1,3) and branched (β-1,3/β-1,6) glycosidic bonds. Complementing the biochemical analysis, we performed an *in silico* modeling of the *Egr*GH64 three-dimensional structure for a deeper understanding of the enzymatic behavior of the enzyme. This study contributes to this enzyme's functioning and potential utility for biotechnological processes.

2. MATERIALS AND METHODS

2.1. Chemicals

Laminarin, β-1,3/β-1,6-glucans from yeast cell walls (BG-YCW), protein standards, and IPTG were obtained from Sigma-Aldrich. All other reagents were of the highest quality available.

2.2. Polysaccharide substrates preparation

Laminarin and β-glucan yeast cell wall (BG-YCW) were dissolved directly in sodium acetate buffer (50 mM, pH 4.5) for each case reaching 100 mg/ml.

Paramylon was purified from the microalgae. *E. gracilis* cells were collected by centrifugation at 2500 *g* for 5 min and washed thrice with distilled water. Cells were disrupted by sonication for 5 min and then centrifuged. The supernatant was discarded, and the pellet washed first, five times with distilled water, and then three washes more with mixture of hexane:water (1:1). Finally, after washing thrice with distilled water, the paramylon was taken to a stove up to constant weight. The paramylon was resuspended in sodium acetate buffer (50 mM, pH 4.5) 100 mg/ml.

2.3. Bacteria and plasmids

Escherichia coli Top 10 F′ cells (Invitrogen) were used for cloning. The recombinant protein was expressed using the pET28c vector (Novagen) and *E. coli* BL21 (DE3) cells

as hosts (Invitrogen). DNA manipulation, *E. coli* culture, and transformation were performed according to standard protocols.

2.4. Cloning of *gh64* gene from *E. gracilis*

Based on transcriptome information (light_m.63754) from *E. gracilis*[17] and using codon optimization for heterologous expression in *E. coli* cells, the gene coding for a putative GH64 from *E. gracilis*(*egrgh64*) was *de novo* synthesized (BIO BASIC INC). The *egrgh64* was designed to be flanked with *Nde*I and *Hind*III restriction sites for later cloning and expression in *E. coli* cells. The pUC57 plasmid harboring the *egrgh64* gene was digested with *Nde*I and *Hind*III. The released gene was separated in a 1% (w/v) agarose gel electrophoresis and purified using a Wizard SV gel & PCR Clean-Up kit (Promega). The digested *egrgh64* gene was subcloned into pET28c to obtain the construct [pET28c/*egrgh64*], including an N-terminal His-tag. This construct was used to transform *E. coli* BL21 (DE3) competent cells.

2.5. Protein production and purification

E. coli BL21 (DE3) cells transformed with [pET28c/*egrgh64*] were grown at 37°C in a TB medium supplemented with 50 μg.ml^{-1} kanamycin and 3% (v/v) ethanol until reaching an OD_{600} ~ 1.0. The *egrgh64* expression was induced with 1.0 mM IPTG at 25°C for 16 h. Centrifugation for15 min at 4°C and 5,000 × *g* served for harvesting the cells. The pellet was suspended in 5 ml of buffer A (25 mM Tris–HCl pH 8.0, 300 mM NaCl, 5% (v/v) glycerol, 10 mM imidazole) per g of cells. Cells were disrupted after sonication on ice and centrifuged at 16,000 × *g* for 20 min at 4°C. *Eg*rGH64 was purified by immobilized metal affinity chromatography (IMAC) using 1 ml HisTrap^{TM} HP columns (GE Healthcare). Briefly, supernatants were loaded onto previously equilibrated Ni^{2+} charged columns. After extensive washing with buffer A, samples

were eluted with a 10 – 300 mM imidazole linear gradient (50-column volumes). Active fractions enriched in *Egr*GH64 were pooled and further purified by gel filtration chromatography. Briefly, the sample was loaded onto a Superdex G-200 column (GE Healthcare) and eluted with buffer A without imidazole. Active fractions were concentrated and supplemented with glycerol (25% v/v). All proteins were stable for at least three months when stored at -80ºC under these conditions.

2.6. Protein methods

Protein concentration was determined by the Bradford procedure [22] using bovine serum albumin as a standard. Proteins were analyzed by SDS-PAGE (in the presence or absence of a reducing agent) according to Laemmli[23] [polyacrylamide monomer concentration was 12% (w/v) for the separating gel and 4% (w/v) for the stacking gel]. Coomassie Brilliant Blue served for protein staining.

2.7. Molecular mass determination

The quaternary structure of the pure recombinant *Egr*GH64 was determined by gel filtration chromatography. The sample was loaded in a Superdex Tricorn 10/300 column (GE Healthcare) in buffer G (50 mM HEPES–NaOH pH 8.0, 100 mM NaCl, and 0.1 mM EDTA). The molecular mass was calculated using a calibration plot constructed with protein standards from GE Healthcare, including thyroglobulin (669 kDa), ferritin (440 kDa), aldolase (158 kDa), conalbumin (75 kDa), ovalbumin (44 kDa), carbonic anhydrase (29 kDa), and ribonuclease A (13.7 kDa). The column void volume was measured using a dextran blue loading solution (Promega).

2.8. Enzyme assay

The standard assay for endo-β-1,3-glucanase activity was performed using 2.5 $mg.ml^{-1}$ laminarin as substrate and a proper enzyme dilution, at 50°C in buffer sodium acetate 50 mM, pH 4.5. After 30 min of reaction, reducing sugars released from laminarin were determined by the Somogyi-Nelson method[24,25]. The substrate consumption was maintained below 10% as a control to ensure the proper determination of the initial rate (v_i). One unit (U) of enzyme activity is defined as the amount of enzyme that catalyze the release of 1 µmol of glucose equivalent released per minute under the assay condition specified above.

The optimal pH of *Egr*GH64 was determined by measuring the hydrolytic activity under the above-specified conditions, except for the different pH values in the assay. The buffers (50 mM) used for these assays contained sodium acetate (pH 3.5, 4.5 and 5.0), sodium phosphate (pH 6.0 and 7.5), or Tris-HCl (pH 8.5, 9.0 and 9.5). Ditto, for measuring optimal temperature, enzyme activity was measured between 15ºC and 65ºC in 50 mM sodium acetate buffer, at pH 4.5. The thermal stability of *Egr*GH64 was measured by determining residual hydrolytic activity at 50°C of the enzyme preincubated for 30 min at different temperatures between 15ºC and 70ºC.

The effect of metal ions was determined by measuring enzymatic activity in the presence of different metal ions (Ni^{2+}, Fe^{3+}, Mn^{2+}, Mg^{2+}, Co^{2+}, Zn^{2+}, and Ca^{2+}) at 5 mM in 50 mM sodium acetate buffer, at pH 4.5.

2.9. Kinetic analysis

We used the approach developed for interfacial enzyme kinetics[26,27], applying two models: the conventional Michaelis-Menten (^{conv}MM) and the inverse Michaelis-Menten(^{inv}MM).Using the ^{conv}MM model, a fixed amount of enzyme activity is assayed

as a function of substrate saturation fitting the data to Equations 1 (where k_{cat} is the turnover number).

$$v = \frac{k_{cat} E_0 S_0}{K_M + S_0} \quad (1)$$

The^{inv}MM approach swaps the role of substrate and enzyme, measuring initial rates at a fixed substrate level and with different enzyme concentrations, according to Equation2.

$$v = \frac{k_{cat} S_0 E_0}{{}^{enz}_{1}K_M + E_0} \quad (2)$$

As in Equation 3, the ratio of parameters, allows determining the density of enzyme attack sites on the polymer substrate surface, where the $^{mass}K_M$ is the parameter corresponding to $^{inv}K_M$ in molar units.

$$\Gamma = \frac{{}^{inv}K_M}{{}^{mass}K_M} = \frac{mol/L}{g/L} \quad (3)$$

The v_i determination for conventional Michaelis-Menten (^{conv}MM) was made with 0.16, 0.26 and 0.19 mg.ml^{-1} of *Egr*GH64 for laminarin, paramylon and BG-YCW respectively. Substrate saturation curve was performed using 2.5, 5.0, 10, 20, 40, 60 and 80 mg. mL^{-1} of each polysaccharide. In the case of inverse Michaelis-Menten (^{inv}MM), the v_i determination was made with 2.5 mg.ml^{-1} substrate and enzyme concentrations between 0.1 µM and 8.7 µM.

All kinetic constants are the mean of at least three independent data sets, reproducible within ±10%. The fitting was done in GraphPad Prism Software (GRAPH PAD Software Inc, California, USA).

2.10. Bioinformatics and molecular modeling

A three-dimensional model of the *Egr*GH64 sequence (EC:3.2.1.39) was obtained using the AlfaFold2 program [28], which employs a deep learning method that has demonstrated a higher accuracy than most modelers [29]. The models' reliability was assessed using the plDDT score, which is returned as part of the results by the AlphaFold2 program. The lDDT[30] values represent a measure of the local similarity that our model would have if compared to the experimentally solved native protein. A value of 100 indicates that the peptide skeleton of our model would likely have the same structure as the native protein if the native protein were experimentally solved. In general, plDDT score values greater than 70 indicate that the model backbone is reliable[29].

The UCSF-Chimera program [31] was used to perform the structural alignment, using a Needleman-Wunst global alignment as an initial guide, with a Blosum62 scoring matrix and an extra penalty to take into account the secondary structure of each molecule. From the structural alignment of all the sequences, a sequence alignment was obtained by placing in columns those residues whose alpha carbons were less than 5 angstroms from each other in some of the homologous sequences.

The sequence and sequence alignment images were obtained using the ESpript 3.0 program implemented in the ESPript server (https://espript.ibcp.fr).

Electrostatic potential maps were calculated for each molecule by solving the Poisson-Boltzmann equation implemented in the APBS (Adaptive Poisson-Boltzmann Solver-[32]) program. The default values for the atom charge were taken from Amber Forcefield. Besides, we fixed the salt concentration (0.0), the temperature (298.150), the inner dielectric of the protein (2.0), and the outer dielectric (78.54) were used. This

potential was projected onto the solvent-excluded surface (SES) using UCSF-Chimera software with a 1.4 Angstroms probe.

2.11. TLC Assay

The degradation of laminarin or paramylon catalyzed by *Egr*GH64 was performed as previously described [33]. Briefly, the reaction mixture (250 µL) was prepared with 0.1% (w/w) laminarin or paramylon in sodium acetate buffer (50 mM, pH 4.5) and 0.16 $mg.ml^{-1}$ purified *Egr*GH64. At different times, 50 µL of the reaction mixture was taken and incubated for 10 min at 100°C for the TLC analysis. Samples were spotted on silica gel 60 F254 plates (Merck, Darmstadt, Germany) and separated using ethyl acetate, acetic acid, and water (2:2:1, v/v) as running solvent. The products were visualized after spraying the plate with a developing reagent (25 mg of orcinol, 9.5 mL of ethanol absolute, and 0.5 ml of sulfuric acid 98%). All the mixture was heated at 100ºC for 5 min before use.

2.12. Processivity assay

The assays for analyzing the distribution of reducing sugars between the insoluble and soluble fractions were performed by digesting paramylon (25 $mg.ml^{-1}$) using 0.25 $U.ml^{-1}$ of enzyme per reaction. After 90 min, the reaction was stopped by incubation at 100°C for 10 min, and the supernatant was removed by centrifugation at 10,000 × *g* for 5 min. The insoluble polysaccharide was washed thrice with 50 mM acetate buffer pH 4.5. The washed paramylon was resuspended in a buffer, and reducing sugars were measured in both fractions with the Somogyi-Nelson method. These data were used to calculate the soluble/insoluble reducing sugar ends ratio [34].

2.13. Anti-fungal Assay

Kluyveromyces lactis GG799 (New England Biolabs) was cultivated in 30 mL of YPD medium (1.0% yeast extract, 2.0% peptone, and 2.0% dextrose) at 30ºC for 24 h. The yeast cells were prepared as previously reported [35]. Briefly, the cells were harvested by centrifugation (10,000 × *g* for 10 min), and the cell pellet was resuspended in 1 ml of sterile distilled water to an OD_{600} of 0.5. An aliquot of the diluted cell suspension was diluted 10^4-fold, and then incubated with several *Egr*GH64 concentrations (0.5, 1.0, 2.0, and 4.0 $mg.ml^{-1}$) in a 50 mM sodium citrate buffer (pH 4.5) at 50°C for 2 h. The degree of fungal growth inhibition was assessed by counting the number of colonies formed on YPD agar plates. Colony counting was performed with the Icy software [36].

3. RESULTS AND DISCUSSION

3.1. Enzyme production, purification, and biochemical properties

In the transcriptome project of *E.gracilis*[17], we found an amino acid sequence corresponding to a putative endo-β-1,3-glucanase (*Egr*GH64). We designed by back translation a gene-based on *E. coli* codon usage (*egrgh4*) for molecular cloning and heterologous expression. The production of recombinant *Egr*GH64 was carried out in *E. coli* BL21 (DE3) host system. Although the protein was primarily produced as inclusion bodies, we improved its folding by supplementing the culture media with 3% (v/v) ethanol. The alcohol stresses the cells and induces the expression of native chaperones [37], generating conditions to obtain the recombinant enzyme (with a histidine-tag at the N-terminus) in soluble form showing activity in its hydrolytic function. After two-step purification, including immobilized metal affinity chromatography (IMAC) and preparative gel filtration chromatography, about 0.6 mg of *Egr*GH64 was purified from

1 L of culture. The purified enzyme exhibited a specific activity (to hydrolyze laminarin) of 0.5 $U.mg^{-1}$. The *Egr*GH64 (predicted Molecular Mass: 65 kDa) migrated as a major single band of ≈66 kDa on SDS-PAGE (Fig. 1A), suggesting a purity higher than 80%. The analysis by size exclusion chromatography showed a monomeric arrangement of *Egr*GH64 (Fig. 1B), which agrees with that reported for members of the GH64 family from different organisms[38,39].

To determine accurate conditions for the functional hydrolytic activity of *Egr*GH64, we searched for the effect of temperature and pH. The enzyme displayed maximal β-1,3-glucanase activity on laminarin at pH 4.5 in 50 mM acetate buffer (Fig. 2A). The optimal temperature for the reaction was found at 50°C, decreasing the enzyme activity by~40% at both 40°C and 60°C (Fig. 2B). Studies on the protein stability showed that *Egr*GH64 was stable up to 50°C, remained more than 80% active when preincubated in the range of 30ºC - 55ºC (Fig. 2C). Besides, from the slope of a linear Arrhenius plot of the activity data in the latter temperature range, a value of energy of activation (E_a) of 56.6 kJ/mol was calculated for the reaction of hydrolysis under enzymatic catalysis (Fig. 2D). We also determined the effects of metal ions (at the concentrations of 5 mM) on *Egr*GH64 activity. We found that Ni^{2+} and Mg^{2+} slightly inhibited *Egr*GH64 activity, while Fe^{3+}, Co^{2+}, Zn^{2+}, and Mn^{2+} showed a marked inhibition (Fig. 2E). Conversely, the enzyme catalysis was not significantly affected by the presence of Ca^{2+}.

3.2. Enzymatic Characterization

A screening of the substrate specificity of purified *Egr*GH64 indicated it exhibited specificity to catalyze the hydrolysis of β-1,3-glycosidic linkages. Thus, the enzyme was active with laminarin, paramylon, and β-glucan from the yeast cell wall (BG-YCW) but neither with carboxymethylcellulose nor cellulose (data not shown). This result

prompted us to characterize in detail the kinetic properties of *Egr*GH64 through the ^{conv}MM and the ^{inv}MM approaches, to obtain data detailed in Figure 3 and Table I. As shown, the saturation kinetics concerning the three substrates was hyperbolic, with the enzyme exhibiting a lower (by one order of magnitude) K_M toward BG-YCW relative to the other two polysaccharides (Fig. 3A). Besides, the higher k_{cat} was reached for laminarin, although the catalytic efficiency for using substrates ordered BG-YCW>laminarin>paramylon (Table I). To better complement this latter information that emerged from the ^{conv}MM analysis based on a substrate excess, it was worth considering that *Egr*GH64 works on polysaccharides. The enzymatic degradation of a polymeric (with relatively low solubility) substrate represents a more complex system with interfacial (near-) heterogeneous characteristics, where a "double saturation" takes place. Indeed, the maximal rate reaches after the substrate and the enzyme saturate each other[26,27]. In the accompanied ^{inv}MM study, we observed that lower enzyme concentrations were necessary to saturate BG-YCW than paramylon and laminarin (Fig. 3B). Consequently, the Γ parameter (which reveals the ability of an enzyme to locate catalytically competent sites on the substrate surface,[26,27] determined for the former polysaccharide was one order of magnitude higher (Table I, and Fig. 3C). Although is hard to compare K_M with $^{enz}K_M$, since these parameters represents saturation of enzymes with substrates or vice versa, they provide information concerning the interaction between the protein with the polymeric (having uncertain molecular size) substrate. In this scenario, our results can be analized considering the higher molecular mass of paramylon (≈600 kDa) compared to the BG-YCW (27-175 kDa), and laminarin (3.5-5.5 kDa), with a decrease in the former of catalytically competent sites per gram of polymer [40,41].

347 The products of the *Egr*GH64 hydrolytic activity on laminarin (Fig. 4A) and paramylon
348 (Fig. 4B) were analyzed by TLC. Results in Figure 4 indicate that, for both substrates,
349 laminaripentaose is the major and smallest product after three hours of reaction.
350 According to previous characterization studies of the endo-glucanases [34,42–45],
351 processivity can be evaluated measuring, after hydrolysis, the ratio between reducing
352 ends concentration present in the soluble fraction / reducing ends concentration present
353 in the insoluble fraction. Non-processive endo-glucanases have a random cutting action
354 leading to a ratio near 1. In contrast, processive endo-glucanases cut only from the ends
355 of the polysaccharide, generating a higher concentration of reducing sugar increasing
356 the ratio. In our case, the soluble/insoluble ratio was 7.5 (Fig. 5), which is consistent
357 with a processive-acting glucanase[46].
358
359 **3.3. Antifungal Assay**
360 Several endo-β-1,3-glucanases can hydrolyze β-1,3-polysaccharides of the fungal cell
361 wall, inhibiting the growth of pathogenic species **[47]**. Since β-1,3-glucans are the main
362 component of the cell wall of many fungi **[48–50]**, we considered *K. lactis* an
363 appropriate organism model to test the above-described hydrolytic activity on BG-
364 YCW, thus evaluating a possible inhibitory effect of *Egr*GH64 on fungal growth. To
365 search in such a way, we incubated *K. lactis* with different enzyme concentrations,
366 observing that the yeast growth was substantially inhibited by *Egr*GH64 in a
367 concentration-dependent manner (Fig 6). The degree of growth inhibition at a
368 concentration of 0.5 mg/ml was ~60% concerning the control. Moreover, the enzyme
369 inhibited more than 90% of the yeast growth at 1 mg/ml (15.4 µM). In this regard,
370 studying this antifungal effect in human pathogenic organisms would be interesting.
371

3.4. GH64 Molecular Modeling

To make a structural comparison with other glucanases, we predicted its putative structure using AlphaFold2. The reliability value plDDT (predicted local Distance Difference Test) shows that more than 86% (517 residues out of 596) of the sequence could be modeled reliably (plDDT>= 70) (Fig. 1 in supplemental data**)**. Figure 7A shows the backbone of the obtained model represented with ribbons and colored according to the plDDT values per residue: residues with scores higher than 70 were colored in blue, and the rest in red. In Figure7B, the three domains that characterize endoglucanases can be observed, two of them forming the characteristic crescent-shaped catalytic region (in red and blue), and one domain with a folding similar to that from carbohydrate-binding modules (CBM), in pink [51]. Figure 7C shows the sequence of GH64 with residues colored according to the domain to which they belong. These boundaries emerged from the structural alignment between the models and the annotated structure in PDBsum of the enzyme from *Streptomyces matensis* (3GD0), [52]**)**. Amino acid residues reported in other endo-β-1,3-glucanases as essentials for the catalytic activity were highlighted with a blue box and a blue triangle below them. The N-terminal region (first fifty amino acid residues) of the best molecular model of *Egr*GH64 was shown to be unreliable predicted (less than 70% plDDT). The predictions of intrinsically disordered regions [53] and signal peptide (SignalP 6.0 and Phobius) [54,55] for that region were negative, unlike the N-terminus of GH64 from *S. matensis* which was predicted as a signal peptide and excluded in its analysis by the authors[52].

3.5. Structure-based sequence alignments

We first performed an alignment of four GH64 sequences: *Euglena gracilis* GH64 (this work), *Streptomyces matensis* GH64 (PDB ID: 3GD0); *Paenibacillusbarengoltzii*GH64

(PDB ID: 5H9X); and *Clostridium beijerinckii* GH64 (PDB ID: 5H4E). Above and below the sequence alignment, the secondary structure corresponding to *E. gracilis* and *S. matensis* is shown schematically (Fig. 8). The numbering in the upper rule corresponds to the sequence of *E. gracilis*, and the blue stars point out the residues that have been described as critical for glucanase activity [52] (Table 1 in supplemental data). The residues that are not only identical but also spatially close (same column) are highlighted in red, giving more relevance to their possible role in the structure of these enzymes. Residues in columns with high sequence similarity are highlighted with blue square rectangles. There are regions with high structural similarity evidenced as blocks of residues in columns without gaps. But there are also some areas with low structural similarity despite being composed of the same secondary structure (red square). Thus, this *in silico* approach allowed us to identify in *Egr*GH64 the presence, in a suitable spatial positioning, of several amino acid residues essential for endo-β-1,3 glucanase activity [52].

3.6. Binding site

Figure 9A (1 - 4) shows the electrostatic potential surface of fourenzymes of the GH64 family: *Euglena gracilis* model (A1), *Streptomyces matensis* (PDB ID: 3GD0, A2); *Clostridium beijerinckii* (PDB ID: 5H4E, A3); *Paenibacillus barengoltzii* (PDB ID: 5H9X, A4). All proteins are shown looking directly at the binding cleft. The region of the catalytic groove (marked with a blue box) is negative (red color) in all enzymes, even with some differences due to different structural characteristics in each molecule. This feature was also observed in mannose-specific lectins [56]. The enzyme from *S. matensis* was previously co-crystallized with a laminaritetraose (PDB ID: 3GD9) [52] positioned in the catalytic cleft. This structural information was a valuable guide for

422 modeling the positioning of this oligosaccharide in the enzymes from *E. gracilis*, *C.*
423 *beijerinckii*, and *P. barengoltzii*. This analysis showed that the substrate could be bound
424 and stabilized in this negatively charged region of the molecules.
425 Figure 9B (1 - 4) depicts the backbone of each enzyme shown in ribbons. The atoms of
426 the amino acid side chains are shown with balls and sticks. Residues described as part
427 of the active site, and structurally conserved are labeled with background colors that
428 allow identification of their position within the structure. It is highlighted that all
429 arrangements present a region with aromatic residues presumably to stabilize the
430 incoming polysaccharide chain (circled in black dashed line). When looking at the
431 3GD9 structure (*S. matensis*) co-crystallized with a lamiraritetraose at the active site, it
432 is visualized that one of the glucose units binds, forming a π-stacking type pairing with
433 tryptophan 163. Also, worth to point out that the *Egr*GH64 model has an additional
434 aspartic acid (D188, circled in red dashed line) in the catalytic pocket. This residue is
435 absent in the other enzymes, structurally close to glutamic acid (E177), which could
436 generate a potentially favorable environment for binding Mn^{2+} ions, affecting the
437 binding of the substrate and explaining the loss of activity in the presence of the metal
438 ion.
439

440 ## 4. CONCLUSIONS

441 A transcript coding for a putative endo-β-1,3-glucanase was identified in the
442 transcriptome of *E. gracilis* (light_m.63754)[17]. The gene *egrgh64* was synthesized *de*
443 *novo* to produce heterologously in *E. coli* BL21(DE3) the recombinant
444 enzyme *Egr*GH64 with a histidine tag at the amino terminus. The protein
445 chromatographically purified exhibited activity on laminarin, paramylon, and BG-
446 YCW. Optimal reaction conditions were established in pH 4.0–5.0, and 50ºC.

Compared to an orthologue enzyme from *S. matensis*, *Egr*GH64 shares structural domains and amino acid residues previously described as critical for catalytic function. The enzyme catalytic efficiency using the different substrates followed the pattern paramylon<laminarin<BG-YCW, although laminaripentaose was the main product of hydrolysis independently of the polysaccharide. The high performance of *Egr*GH64 was found consequent with an elevated density of hydrolysis sites in the β-1,3/β-1,6-glucan. Results on protein structure modeling detailed herein give insights into the β-1,3-glucanase functionality of the enzyme. Studies are on the way to further analyze the interaction of *Egr*GH64 with the substrate, to understand structural clues determining varied preferences to hydrolyze β-glucans with different polymerization and/or branching degrees.

*Egr*GH64 is the first functional endo-β-1,3-glucanase from *E. gracilis* produced recombinantly using a prokaryote host system. Previously, a GH17 protein from *E. gracilis* was successfully expressed in *Aspergillus oryzae* (Takeda et al., 2015). Its characterization supports that, *in vivo*, it would be involved in the metabolism of paramylon. Indeed, the enzyme could participate in initiating the polyglucan degradation to a minor degree but with a higher contribution in further hydrolyzing laminarin released by other glucanases. The identification and characterization of *Egr*GH64 provide biotechnological instruments for future industrial applications. Thus, considering its ability to strongly inhibit the growth of *K. lactis* in a dose-dependent mode, the enzyme could be evaluated as a molecular tool, as an anti-fungal agent, against human pathogen strains of the genus *Candida* or different strains of dermatophytes. Besides, the *Egr*GH64 activity could also serve as a tool in generating musts enriched in reducing sugar after degradation of β-1,3- or β-1,3/β-1,6-glucan.

471

AUTHOR STATEMENT

R. D. Calloni: Conceptualization, Methodology, Software, Formal analysis, Investigation, Writing - Original Draft, Visualization. **R. J. Muchut**:Methodology.**S. E. Garay**:Software, Writing-OriginalDraft,Visualization.**D. G. Arias**:Methodology, Formal analysis. **A. A. Iglesias**: Writing - Review & Editing, Funding acquisition. **S. A. Guerrero**: Conceptualization, Formal analysis, Writing - Review & Editing, Supervision, Project administration, Funding acquisition.

ACKNOWLEDGMENTS

We thank Dr. Robert Field (Manchester Institute of Biotechnology, UK) and Dr. Ellis O´Neill (University of Nottingham, UK), for kindly share information about transcriptome of *E. gracilis*. DGA, AAI and SAG are investigator career members from CONICET. RDC and RJM are doctoral and postdoctoral fellows respectively in the same Institution. This work was supported by grants from ANPCyT (PICT 2015-1149, PICT 2016-1110, PICT 2019- 0349).

REFERENCES

[1] B. Zakryś, R. Milanowski, A. Karnkowska, Evolutionary Origin of Euglena, Adv Exp Med Biol. 979 (2017) 3–17. https://doi.org/10.1007/978-3-319-54910-1_1.

[2] S.A. Breglia, N. Yubuki, M. Hoppenrath, B.S. Leander, Ultrastructure and molecular phylogenetic position of a novel euglenozoan with extrusive episymbiotic bacteria: Bihospites bacati n. gen. et sp. (Symbiontida), BMC Microbiol. 10 (2010) 145. https://doi.org/10.1186/1471-2180-10-145.

[3] G.I. McFadden, Origin and evolution of plastids and photosynthesis in eukaryotes, Cold Spring Harb Perspect Biol. 6 (2014) a016105. https://doi.org/10.1101/cshperspect.a016105.

[4] N. Yubuki, V.P. Edgcomb, J.M. Bernhard, B.S. Leander, Ultrastructure and molecular phylogeny of Calkinsia aureus: cellular identity of a novel clade of deep-sea euglenozoans with epibiotic bacteria, BMC Microbiol. 9 (2009) 16. https://doi.org/10.1186/1471-2180-9-16.

[5] T.E. Ebenezer, R.S. Low, E.C. O'Neill, I. Huang, A. DeSimone, S.C. Farrow, R.A. Field, M.L. Ginger, S.A. Guerrero, M. Hammond, V. Hampl, G. Horst, T. Ishikawa, A. Karnkowska, E.W. Linton, P. Myler, M. Nakazawa, P. Cardol, R. Sánchez-Thomas, B.J. Saville, M.R. Shah, A.G.B. Simpson, A. Sur, K. Suzuki, K.M. Tyler, P.V. Zimba, N. Hall, M.C. Field, Euglena International Network (EIN): Driving euglenoid biotechnology for the benefit of a challenged world, Biology Open. 11 (2022) bio059561. https://doi.org/10.1242/bio.059561.

[6] L. Barsanti, P. Gualtieri, Paramylon, a Potent Immunomodulator from WZSL Mutant of Euglena gracilis, Molecules. 24 (2019) E3114. https://doi.org/10.3390/molecules24173114.

[7] P. Teerawanichpan, X. Qiu, Fatty acyl-CoA reductase and wax synthase from Euglena gracilis in the biosynthesis of medium-chain wax esters, Lipids. 45 (2010) 263–273. https://doi.org/10.1007/s11745-010-3395-2.

[8] Y.-W. Kim, K.-H. Kim, H.-J. Choi, D.-S. Lee, Anti-diabetic activity of beta-glucans and their enzymatically hydrolyzed oligosaccharides from Agaricus blazei, Biotechnol Lett. 27 (2005) 483–487. https://doi.org/10.1007/s10529-005-2225-8.

[9] T.H. Hida, K. Ishibashi, N.N. Miura, Y. Adachi, Y. Shirasu, N. Ohno, Cytokine induction by a linear 1,3-glucan, curdlan-oligo, in mouse leukocytes in vitro, Inflamm Res. 58 (2009) 9–14. https://doi.org/10.1007/s00011-008-8141-3.

[10] J. Shimizu, M. Oka, K. Kudoh, M. Wada, T. Takita, S. Innami, T. Tadokoro, A. Maekawa, Effects of a partially hydrolyzed curdlan on serum and hepatic cholesterol concentration, and cecal fermentation in rats, Int J Vitam Nutr Res. 72 (2002) 101–108. https://doi.org/10.1024/0300-9831.72.2.101.

[11] J.R. Cook, Photosynthetic Activity during the Division Cycle in Synchronized *Euglena gracilis*, Plant Physiol. 41 (1966) 821–825. https://doi.org/10.1104/pp.41.5.821.

[12] H. Inui, K. Miyatake, Y. Nakano, S. Kitaoka, Wax ester fermentation in *Euglena gracilis*, FEBS Letters. 150 (1982) 89–93. https://doi.org/10.1016/0014-5793(82)81310-0.

[13] A. Gissibl, A. Sun, A. Care, H. Nevalainen, A. Sunna, Bioproducts From Euglena gracilis: Synthesis and Applications, Front. Bioeng. Biotechnol. 7 (2019) 108. https://doi.org/10.3389/fbioe.2019.00108.

[14] J. Fellig, Laminarase of *Euglena gracilis*, Science. 131 (1960) 832–832. https://doi.org/10.1126/science.131.3403.832.

[15] D.R. Barras, B.A. Stone, β1,3-Glucan hydrolases from Euglena gracilis, Biochimica et Biophysica Acta (BBA) - Enzymology. 191 (1969) 329–341. https://doi.org/10.1016/0005-2744(69)90252-6.

[16] D.R. Barras, B.A. Stone, β-1,3-glucan hydrolases from Euglena gracilis, Biochimica et Biophysica Acta (BBA) - Enzymology. 191 (1969) 342–353. https://doi.org/10.1016/0005-2744(69)90253-8.

[17] E.C. O'Neill, M. Trick, L. Hill, M. Rejzek, R.G. Dusi, C.J. Hamilton, P.V. Zimba, B. Henrissat, R.A. Field, The transcriptome of Euglena gracilis reveals unexpected metabolic capabilities for carbohydrate and natural product biochemistry, Mol Biosyst. 11 (2015) 2808–2820. https://doi.org/10.1039/c5mb00319a.

[18] Y. Yoshida, T. Tomiyama, T. Maruta, M. Tomita, T. Ishikawa, K. Arakawa, De novo assembly and comparative transcriptome analysis of Euglena gracilis in response to anaerobic conditions, BMC Genomics. 17 (2016) 182. https://doi.org/10.1186/s12864-016-2540-6.

[19] A. Gissibl, A. Care, A. Sun, G. Hobba, H. Nevalainen, A. Sunna, Development of screening strategies for the identification of paramylon-degrading enzymes, Journal of Industrial Microbiology and Biotechnology. 46 (2019) 769–781. https://doi.org/10.1007/s10295-019-02157-7.

[20] Y. Tanaka, K. Goto, J. Luo, K. Nishino, T. Ogawa, T. Maruta, T. Ishikawa, Identification of glucanases and phosphorylases involved in hypoxic paramylon degradation in Euglena gracilis, Algal Research. 67 (2022) 102829. https://doi.org/10.1016/j.algal.2022.102829.

[21] T. Takeda, Y. Nakano, M. Takahashi, N. Konno, Y. Sakamoto, R. Arashida, Y. Marukawa, E. Yoshida, T. Ishikawa, K. Suzuki, Identification and enzymatic characterization of an endo-1,3-β-glucanase from Euglena gracilis, Phytochemistry. 116 (2015) 21–27. https://doi.org/10.1016/j.phytochem.2015.05.010.
[22] M.M. Bradford, A rapid and sensitive method for the quantitation of microgram quantities of protein utilizing the principle of protein-dye binding, Anal Biochem. 72 (1976) 248–254. https://doi.org/10.1006/abio.1976.9999.
[23] U.K. Laemmli, Cleavage of structural proteins during the assembly of the head of bacteriophage T4, Nature. 227 (1970) 680–685. https://doi.org/10.1038/227680a0.
[24] Y.-K. Kim, Y. Sakano, Analyses of Reducing Sugars on a Thin-layer Chromatographic Plate with Modified Somogyi and Nelson Reagents, and with Copper Bicinchoninate, Bioscience, Biotechnology, and Biochemistry. 60 (1996) 594–597. https://doi.org/10.1271/bbb.60.594.
[25] A. Storani, S.A. Guerrero, A.A. Iglesias, On the functionality of the N-terminal domain in xylanase 10A from Ruminococcus albus 8, Enzyme and Microbial Technology. 142 (2020) 109673. https://doi.org/10.1016/j.enzmictec.2020.109673.
[26] J. Kari, S.J. Christensen, M. Andersen, S.S. Baiget, K. Borch, P. Westh, A practical approach to steady-state kinetic analysis of cellulases acting on their natural insoluble substrate, Anal Biochem. 586 (2019) 113411. https://doi.org/10.1016/j.ab.2019.113411.
[27] J. Kari, M. Andersen, K. Borch, P. Westh, An Inverse Michaelis–Menten Approach for Interfacial Enzyme Kinetics, ACS Catal. 7 (2017) 4904–4914. https://doi.org/10.1021/acscatal.7b00838.
[28] K. Tunyasuvunakool, J. Adler, Z. Wu, T. Green, M. Zielinski, A. Žídek, A. Bridgland, A. Cowie, C. Meyer, A. Laydon, S. Velankar, G.J. Kleywegt, A. Bateman, R. Evans, A. Pritzel, M. Figurnov, O. Ronneberger, R. Bates, S.A.A. Kohl, A. Potapenko, A.J. Ballard, B. Romera-Paredes, S. Nikolov, R. Jain, E. Clancy, D. Reiman, S. Petersen, A.W. Senior, K. Kavukcuoglu, E. Birney, P. Kohli, J. Jumper, D. Hassabis, Highly accurate protein structure prediction for the human proteome, Nature. 596 (2021) 590–596. https://doi.org/10.1038/s41586-021-03828-1.
[29] J. Jumper, R. Evans, A. Pritzel, T. Green, M. Figurnov, O. Ronneberger, K. Tunyasuvunakool, R. Bates, A. Žídek, A. Potapenko, A. Bridgland, C. Meyer, S.A.A. Kohl, A.J. Ballard, A. Cowie, B. Romera-Paredes, S. Nikolov, R. Jain, J. Adler, T. Back, S. Petersen, D. Reiman, E. Clancy, M. Zielinski, M. Steinegger, M. Pacholska, T. Berghammer, S. Bodenstein, D. Silver, O. Vinyals, A.W. Senior, K. Kavukcuoglu, P. Kohli, D. Hassabis, Highly accurate protein structure prediction with AlphaFold, Nature. 596 (2021) 583–589. https://doi.org/10.1038/s41586-021-03819-2.
[30] V. Mariani, M. Biasini, A. Barbato, T. Schwede, lDDT: a local superposition-free score for comparing protein structures and models using distance difference tests, Bioinformatics. 29 (2013) 2722–2728. https://doi.org/10.1093/bioinformatics/btt473.
[31] E.F. Pettersen, T.D. Goddard, C.C. Huang, G.S. Couch, D.M. Greenblatt, E.C. Meng, T.E. Ferrin, UCSF Chimera--a visualization system for exploratory research and analysis, J Comput Chem. 25 (2004) 1605–1612. https://doi.org/10.1002/jcc.20084.
[32] E. Jurrus, D. Engel, K. Star, K. Monson, J. Brandi, L.E. Felberg, D.H. Brookes, L. Wilson, J. Chen, K. Liles, M. Chun, P. Li, D.W. Gohara, T. Dolinsky, R. Konecny, D.R. Koes, J.E. Nielsen, T. Head-Gordon, W. Geng, R. Krasny, G.-W. Wei, M.J. Holst, J.A. McCammon, N.A. Baker, Improvements to the APBS biomolecular solvation software suite, Protein Sci. 27 (2018) 112–128. https://doi.org/10.1002/pro.3280.
[33] T.J. Simmons, S.C. Fry, Bonds broken and formed during the mixed-linkage glucan : xyloglucan endotransglucosylase reaction catalysed by Equisetum hetero-trans-β-glucanase, Biochem J. 474 (2017) 1055–1070. https://doi.org/10.1042/BCJ20160935.
[34] X.-Z. Zhang, N. Sathitsuksanoh, Y.-H.P. Zhang, Glycoside hydrolase family 9 processive endoglucanase from Clostridium phytofermentans: heterologous expression, characterization, and synergy with family 48 cellobiohydrolase, Bioresour Technol. 101 (2010) 5534–5538. https://doi.org/10.1016/j.biortech.2010.01.152.
[35] L. Bai, J. Kim, K.-H. Son, D.-H. Shin, B.-H. Ku, D.Y. Kim, H.-Y. Park, Novel Anti-Fungal d-Laminaripentaose-Releasing Endo-β-1,3-glucanase with a RICIN-like Domain from Cellulosimicrobium funkei HY-13, Biomolecules. 11 (2021) 1080. https://doi.org/10.3390/biom11081080.
[36] I. Mekterović, D. Mekterović, Z. Maglica, BactImAS: a platform for processing and analysis of bacterial time-lapse microscopy movies, BMC Bioinformatics. 15 (2014) 251. https://doi.org/10.1186/1471-2105-15-251.
[37] G. Chhetri, P. Kalita, T. Tripathi, An efficient protocol to enhance recombinant protein expression using ethanol in Escherichia coli, MethodsX. 2 (2015) 385–391. https://doi.org/10.1016/j.mex.2015.09.005.

[38] Z. Qin, D. Yang, X. You, Y. Liu, S. Hu, Q. Yan, S. Yang, Z. Jiang, The recognition mechanism of triple-helical β-1,3-glucan by a β-1,3-glucanase, Chem Commun (Camb). 53 (2017) 9368–9371. https://doi.org/10.1039/c7cc03330c.

[39] K.L. Shrestha, S.-W. Liu, C.-P. Huang, H.-M. Wu, W.-C. Wang, Y.-K. Li, Characterization and identification of essential residues of the glycoside hydrolase family 64 laminaripentaose-producing-β-1, 3-glucanase, Protein Eng Des Sel. 24 (2011) 617–625. https://doi.org/10.1093/protein/gzr031.

[40] Y. Daglio, M.C. Rodríguez, H.J. Prado, M.C. Matulewicz, Paramylon and synthesis of its ionic derivatives: Applications as pharmaceutical tablet disintegrants and as colloid flocculants, Carbohydr Res. 484 (2019) 107779. https://doi.org/10.1016/j.carres.2019.107779.

[41] B. Du, M. Meenu, H. Liu, B. Xu, A Concise Review on the Molecular Structure and Function Relationship of β-Glucan, Int J Mol Sci. 20 (2019) E4032. https://doi.org/10.3390/ijms20164032.

[42] W. Wang, T. Archbold, J.S. Lam, M.S. Kimber, M.Z. Fan, A processive endoglucanase with multi-substrate specificity is characterized from porcine gut microbiota, Sci Rep. 9 (2019) 13630. https://doi.org/10.1038/s41598-019-50050-1.

[43] A.I. Chiriac, E.M. Cadena, T. Vidal, A.L. Torres, P. Diaz, F.I. Javier Pastor, Engineering a family 9 processive endoglucanase from Paenibacillus barcinonensis displaying a novel architecture, Appl Microbiol Biotechnol. 86 (2010) 1125–1134. https://doi.org/10.1007/s00253-009-2350-8.

[44] K. Lv, W. Shao, M.M. Pedroso, J. Peng, B. Wu, J. Li, B. He, G. Schenk, Enhancing the catalytic activity of a GH5 processive endoglucanase from Bacillus subtilis BS-5 by site-directed mutagenesis, International Journal of Biological Macromolecules. 168 (2021) 442–452. https://doi.org/10.1016/j.ijbiomac.2020.12.060.

[45] B. Wu, S. Zheng, M.M. Pedroso, L.W. Guddat, S. Chang, B. He, G. Schenk, Processivity and enzymatic mechanism of a multifunctional family 5 endoglucanase from Bacillus subtilis BS-5 with potential applications in the saccharification of cellulosic substrates, Biotechnol Biofuels. 11 (2018) 20. https://doi.org/10.1186/s13068-018-1022-2.

[46] S. Wu, S. Wu, Processivity and the Mechanisms of Processive Endoglucanases, Appl Biochem Biotechnol. 190 (2020) 448–463. https://doi.org/10.1007/s12010-019-03096-w.

[47] C.-B. Woo, H.-N. Kang, S.-B. Lee, Molecular cloning and anti-fungal effect of endo-β-1,3-glucanase from Thermotoga maritima, Food Sci Biotechnol. 23 (2014) 1243–1246. https://doi.org/10.1007/s10068-014-0170-9.

[48] R. Garcia-Rubio, H.C. de Oliveira, J. Rivera, N. Trevijano-Contador, The Fungal Cell Wall: Candida, Cryptococcus, and Aspergillus Species, Front. Microbiol. 10 (2020) 2993. https://doi.org/10.3389/fmicb.2019.02993.

[49] K. Backhaus, C.J. Heilmann, A.G. Sorgo, G. Purschke, C.G. de Koster, F.M. Klis, J.J. Heinisch, A systematic study of the cell wall composition of Kluyveromyces lactis, Yeast. 27 (2010) 647–660. https://doi.org/10.1002/yea.1781.

[50] T.H. Nguyen, G.H. Fleet, P.L. Rogers, Composition of the cell walls of several yeast species, Applied Microbiology and Biotechnology. 50 (1998) 206–212. https://doi.org/10.1007/s002530051278.

[51] D. Guillén, S. Sánchez, R. Rodríguez-Sanoja, Carbohydrate-binding domains: multiplicity of biological roles, Appl Microbiol Biotechnol. 85 (2010) 1241–1249. https://doi.org/10.1007/s00253-009-2331-y.

[52] H.-M. Wu, S.-W. Liu, M.-T. Hsu, C.-L. Hung, C.-C. Lai, W.-C. Cheng, H.-J. Wang, Y.-K. Li, W.-C. Wang, Structure, mechanistic action, and essential residues of a GH-64 enzyme, laminaripentaose-producing beta-1,3-glucanase, J Biol Chem. 284 (2009) 26708–26715. https://doi.org/10.1074/jbc.M109.010983.

[53] B. Mészáros, G. Erdos, Z. Dosztányi, IUPred2A: context-dependent prediction of protein disorder as a function of redox state and protein binding, Nucleic Acids Res. 46 (2018) W329–W337. https://doi.org/10.1093/nar/gky384.

[54] J.J. Almagro Armenteros, K.D. Tsirigos, C.K. Sønderby, T.N. Petersen, O. Winther, S. Brunak, G. von Heijne, H. Nielsen, SignalP 5.0 improves signal peptide predictions using deep neural networks, Nat Biotechnol. 37 (2019) 420–423. https://doi.org/10.1038/s41587-019-0036-z.

[55] L. Käll, A. Krogh, E.L.L. Sonnhammer, A combined transmembrane topology and signal peptide prediction method, J Mol Biol. 338 (2004) 1027–1036. https://doi.org/10.1016/j.jmb.2004.03.016.

[56] A. Barre, Y. Bourne, E.J.M. Van Damme, P. Rougé, Overview of the Structure–Function Relationships of Mannose-Specific Lectins from Plants, Algae and Fungi, Int J Mol Sci. 20 (2019) E254. https://doi.org/10.3390/ijms20020254.

664

665 **TABLE I** Kinetic parameters of the *Egr*GH64 using several glucans as
666 substrates. Laminarin (soluble β-1,3 glucan), paramylon (insoluble β-1,3-glucan) and
667 yeast β-Glucan (insoluble β-1,3-1,6-glucan) were analyzed using both ^{conv}MM and
668 ^{inv}MM equations. Data are plot means ± SEM.

669

Substrate	K_M **(mg.ml^{-1})**	k_{cat} **(s^{-1})**	k_{cat}/K_M **(ml.mg^{-1}. s^{-1})**	$^{enz}K_M$**(µM)**	Γ **(µmol/g)**
Laminarin	23.5 ± 3.9	1.20 ± 0,20	0.051 ± 0.006	2.19± 0.63	0.028 ± 0.008
Paramylon	20.2 ± 2.8	0.23 ± 0,09	0.011 ± 0.002	3.89 ± 0.92	0.028 ± 0.03
Yeast β-Glucan	2.1 ± 0.4	0.88 ± 0,07	0.419 ± 0.073	1.50 ± 0.45	0.31 ± 0.12

670

671 **LEGEND TO THE FIGURES**

672 **FIGURE 1:** *Egr*GH64 purification. (A) SDS-PAGE *Egr*GH64 production and
673 purification after IMAC and gel filtration chromatography (predicted Molecular Mass:
674 65kDa). M: Molecular mass marker, 1: *Egr*GH64 purification. (B) Gel filtration
675 chromatography elution profile.

676

677 **FIGURE 2:** Effect of pH, metal ions, temperature, and thermostability on *Egr*GH64
678 enzymatic activity. (A) Effect of pH on *Egr*GH64 activity. Optimal pH was determined
679 by measuring enzyme activity at pH 3.5, 4.5, 5, 6, 7.5, 8, 9.5, and 10. (B) Effect of
680 temperature on *Egr*GH64 activity. The optimal temperature was determined by
681 measuring enzymatic activity at 30, 40, 45, 50, 55, 60, and 70°C. (C) *Egr*GH64
682 thermostability. Activity was measured after pre-incubating the enzyme for 15 min at
683 temperatures between 4 and 70°C. (D) Arrhenius plots determined for *Egr*GH64 from
684 measurements of the activity. (E) The effect of metal ions on *Egr*GH64 activity. The
685 activity of *Egr*GH64 was measured in the presence of various metal ions (5 mM). The
686 error bars represent the SEM of the triplicate measurements.

687

688 **FIGURE 3:** *Egr*GH64 kinetic characterization. ^{conv}MM (A) and ^{inv}MM (B) saturation
689 curves against laminarin (circles, solid line), paramylon (squares, dashed line), and BG-
690 YCW (triangles, dotted line) relativized to the maximum rate measured for each
691 substrate. ^{conv}MM. ^{inv}MM saturation curves were made with 2.5 mg/ml from each
692 substrate. (C) Enzymatic efficiency and attack site density from *Egr*GH64 towards
693 laminarin (black), paramylon (white), and BG-YCW (gray). The error bars represent the
694 SEM (Standard error of the mean) of the triplicate measurements.

695

FIGURE 4: TLC of hydrolysis products by *Egr*GH64 from laminarin (A) and paramylon (B) for 3 h. The reaction mixture containing 25 ($mg.ml^{-1}$) of the substrates in 50 mM sodium acetate buffer (pH 4.5) was incubated with the purified enzyme at 50 °C. **S**, standard marker (**G**, glucose; **L2**, laminaribiose; **L3**, laminaritriose; **L4**, laminaritetraose; **L5**, laminaripentaose; **L6**, laminarihexaose); **1** Incubation for 15 min, **2** 30 min, **3** 60 min, **4** 120 min, **5** 180 min.

FIGURE 5: Distribution of reducing sugars generated by *Egr*GH64 on paramylon. The concentrations of reducing sugars were determined by the Somogyi-Nelson method. The error bars represent the SEM of the triplicate measurements.

FIGURE 6: Inhibition of *K. lactis* growth dependent on *Egr*GH64 concentration. The yeast was incubated with several enzyme concentrations in 50 mM sodium citrate buffer (pH 4.5) at 50°C as described in M&M. (A) Control growth in a plate of *K. lactis* without incubation with *Egr*GH64. (B) Growth in plate of *K. lactis* pre-incubated with *Egr*GH64 (4.0 $mg.ml^{-1}$). (C) Inhibition of growth curve (number of colonies *vs*. *Egr*GH64 concentration).

FIGURE 7: Sequence alignment obtained from the model structural alignment of *Euglena gracilis*, *Streptomyces matensis* (PDB ID: 3GD0); *Paenibacillus barengoltzii* (PDB ID: 5H9X); *Clostridium beijerinckii* (PDB ID: 5H4E). The numbering in the upper rule corresponds to the sequence of *E. gracilis*. Above and below the sequence alignment, the secondary structure corresponding to *E. gracilis* and *S. matensis*,

719 respectively, is shown schematically. Blue stars show the residues described as critical
720 for glucanase activity [52]. In red, residues that are not only identical but also spatially
721 close (same column) are highlighted, giving more relevance to their possible role in the
722 structure of these enzymes. Residues in columns with high sequence similarity are
723 highlighted with square rectangles.

724

725 **FIGURE 8:** Three-dimensional model obtained with AlphaFold2 colored by the plDDT
726 score (A), in blue are colored the residues with plDDT score higher than 70 (reliable),
727 and by the domain (B). Sequence of the *Egr*GH64 model (C). The colors used to
728 highlight the regions of each domain were used correspondingly in the sequence.

729

730 **FIGURE 9:** (A)Electrostatic potential surface of the four enzymes: *Euglena gracilis*
731 model (A1), *Streptomyces matensis* (PDB ID: 3GD0, A2); *Clostridium beijerinckii*
732 (PDB ID: 5H4E, A3); *Paenibacillus barengoltzii* (PDB ID: 5H9X, A4). All proteins are
733 shown looking directly at the binding cleft (B1 to B4). Backbone of the four enzymes
734 shown in ribbons, and the atoms of the amino acid side chains are shown with balls and
735 sticks. Residues described as part of the active site, and structurally conserved are
736 labeled with background colors that allow identification of their position within the
737 structure.

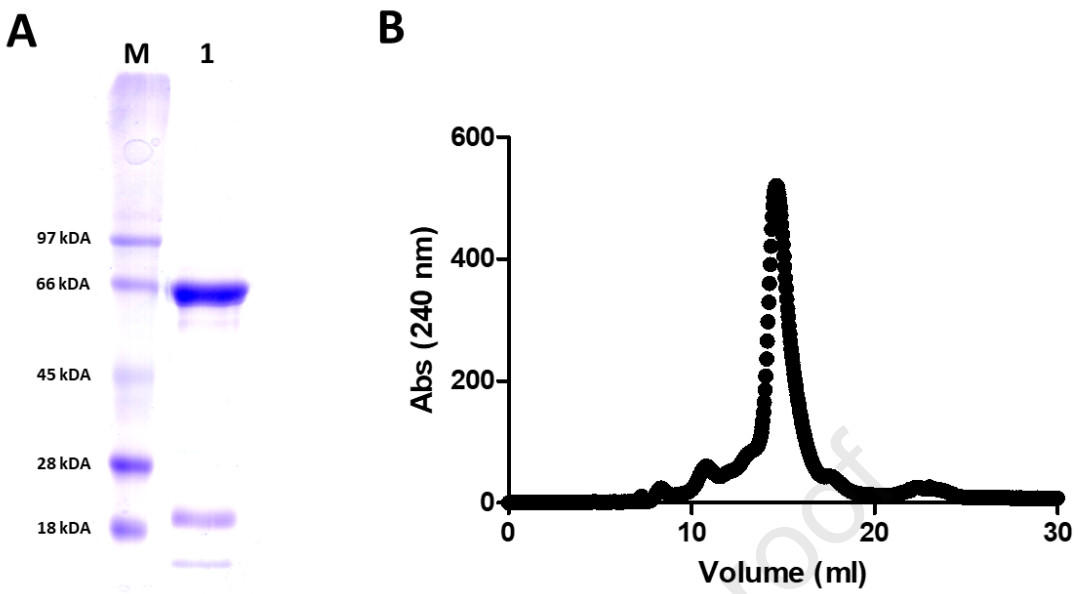

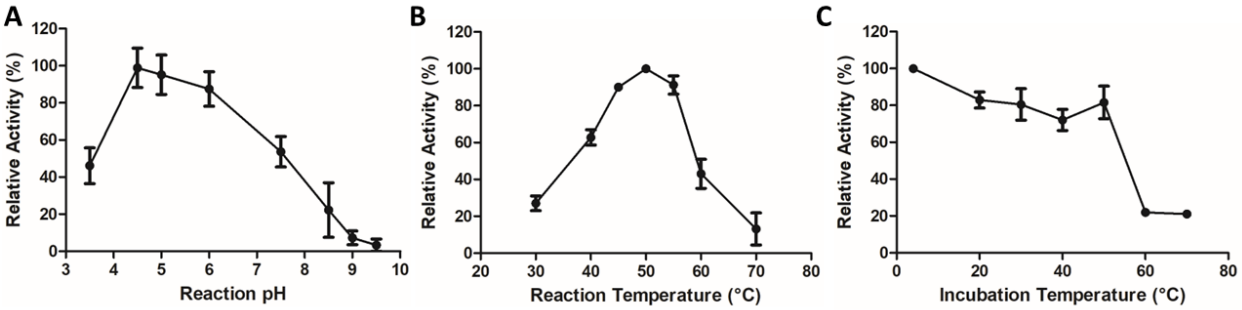

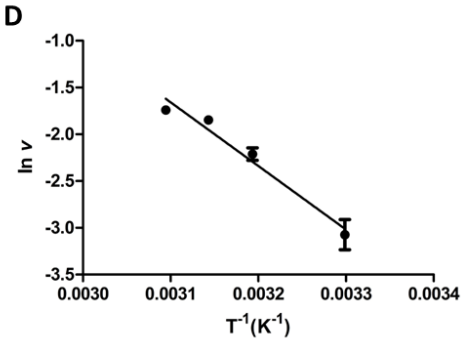

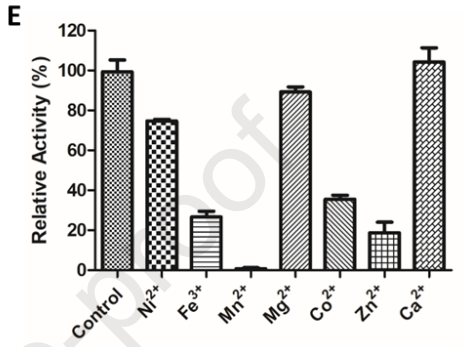

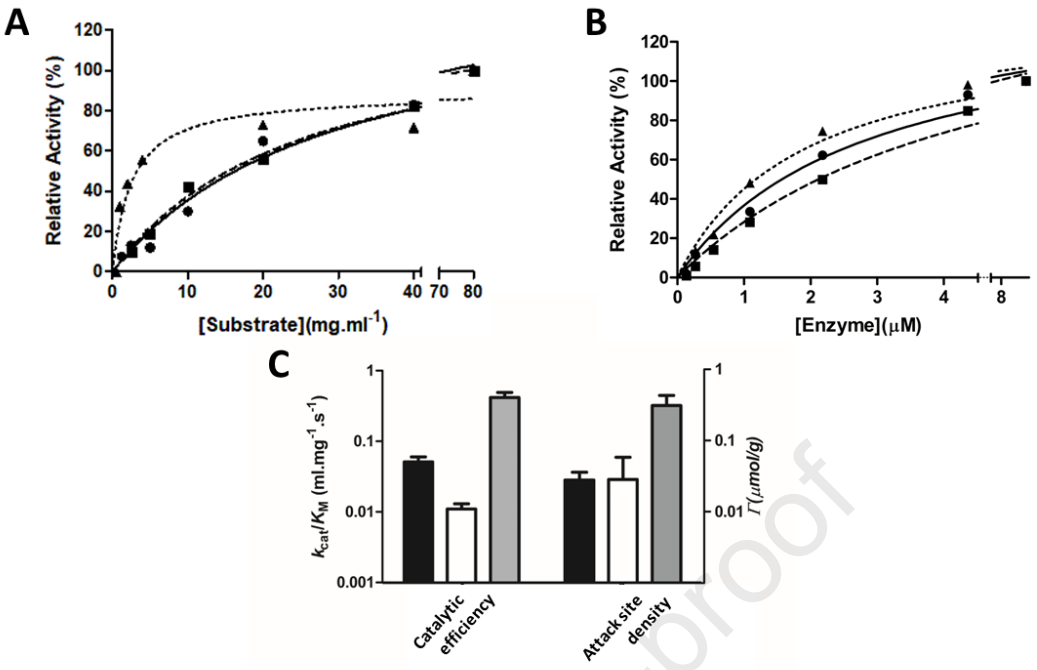

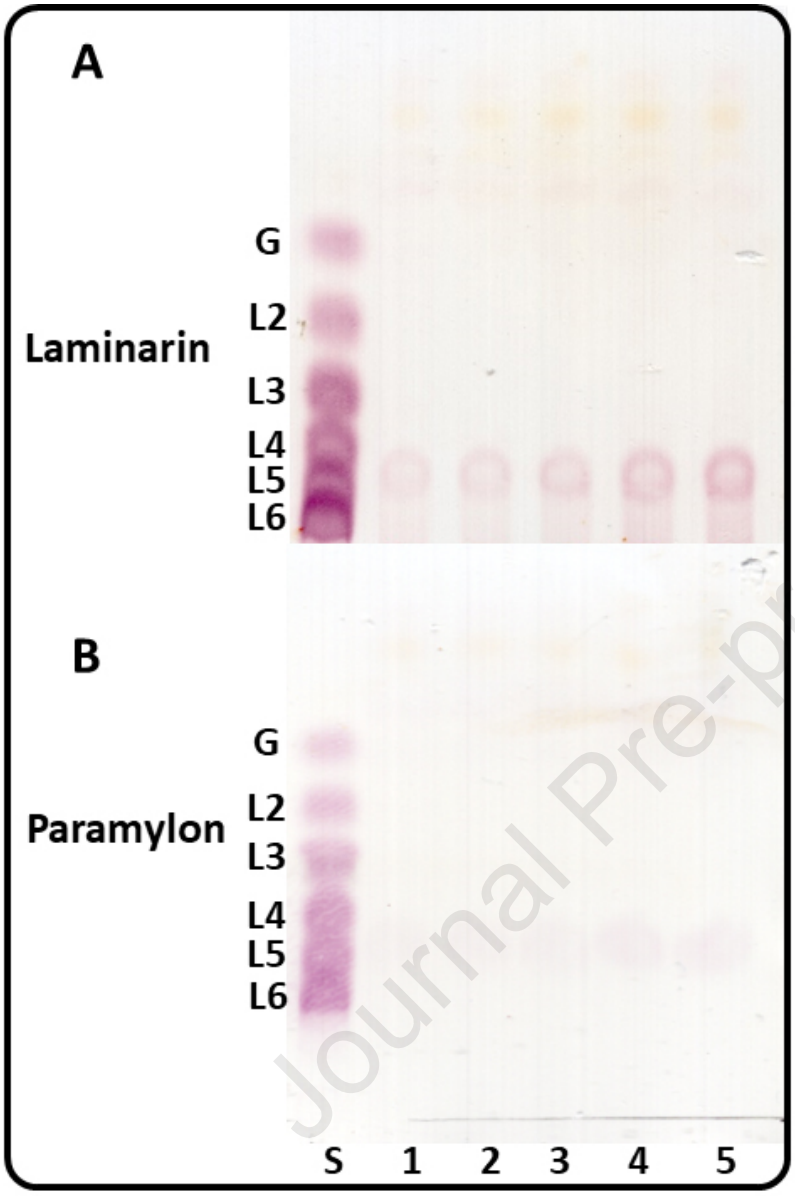

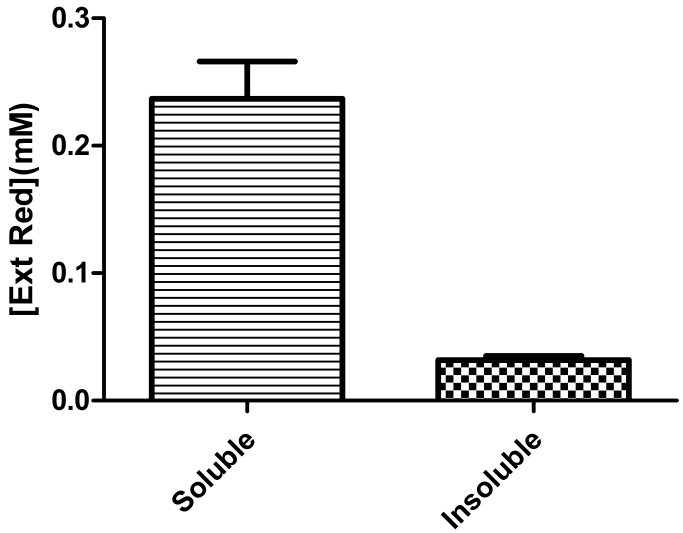

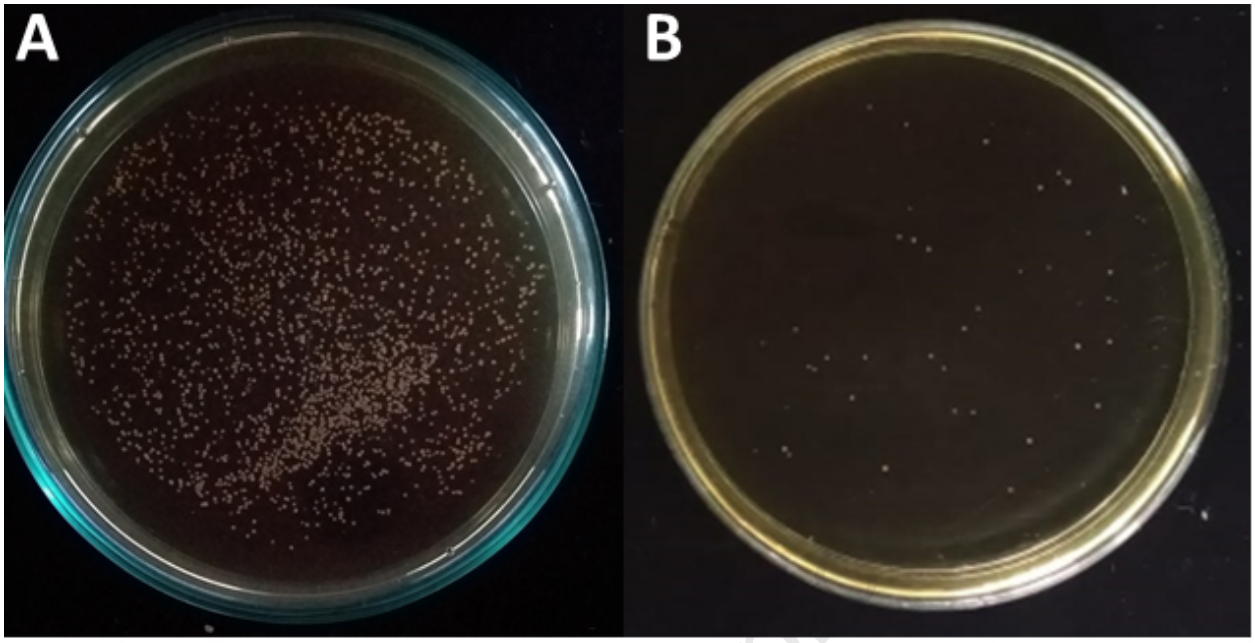

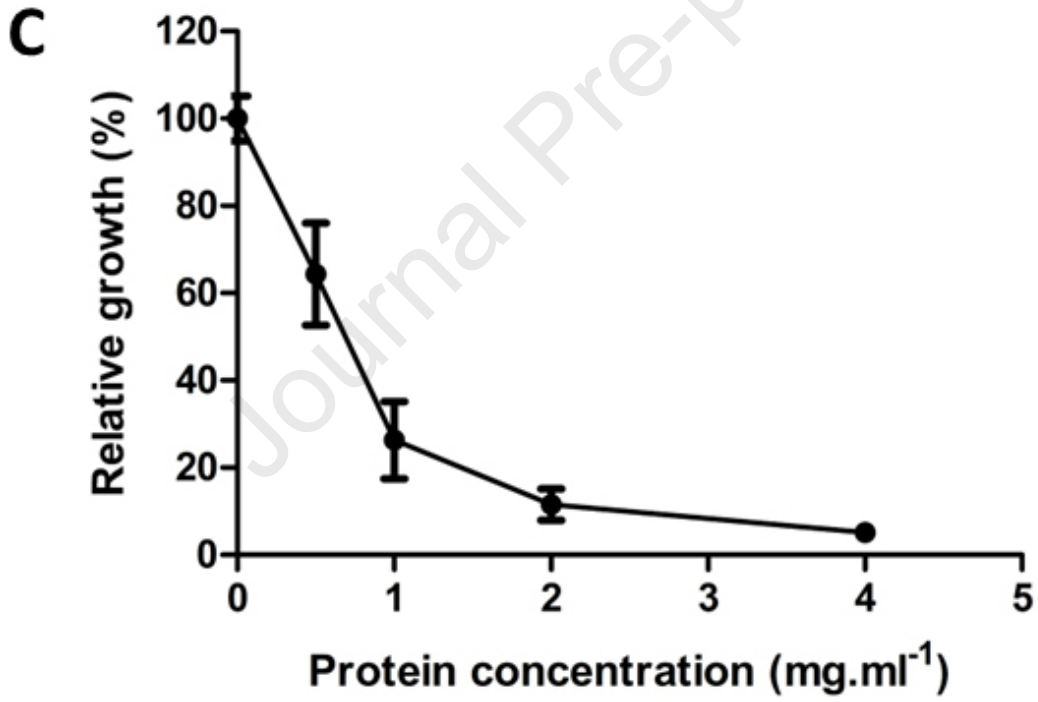

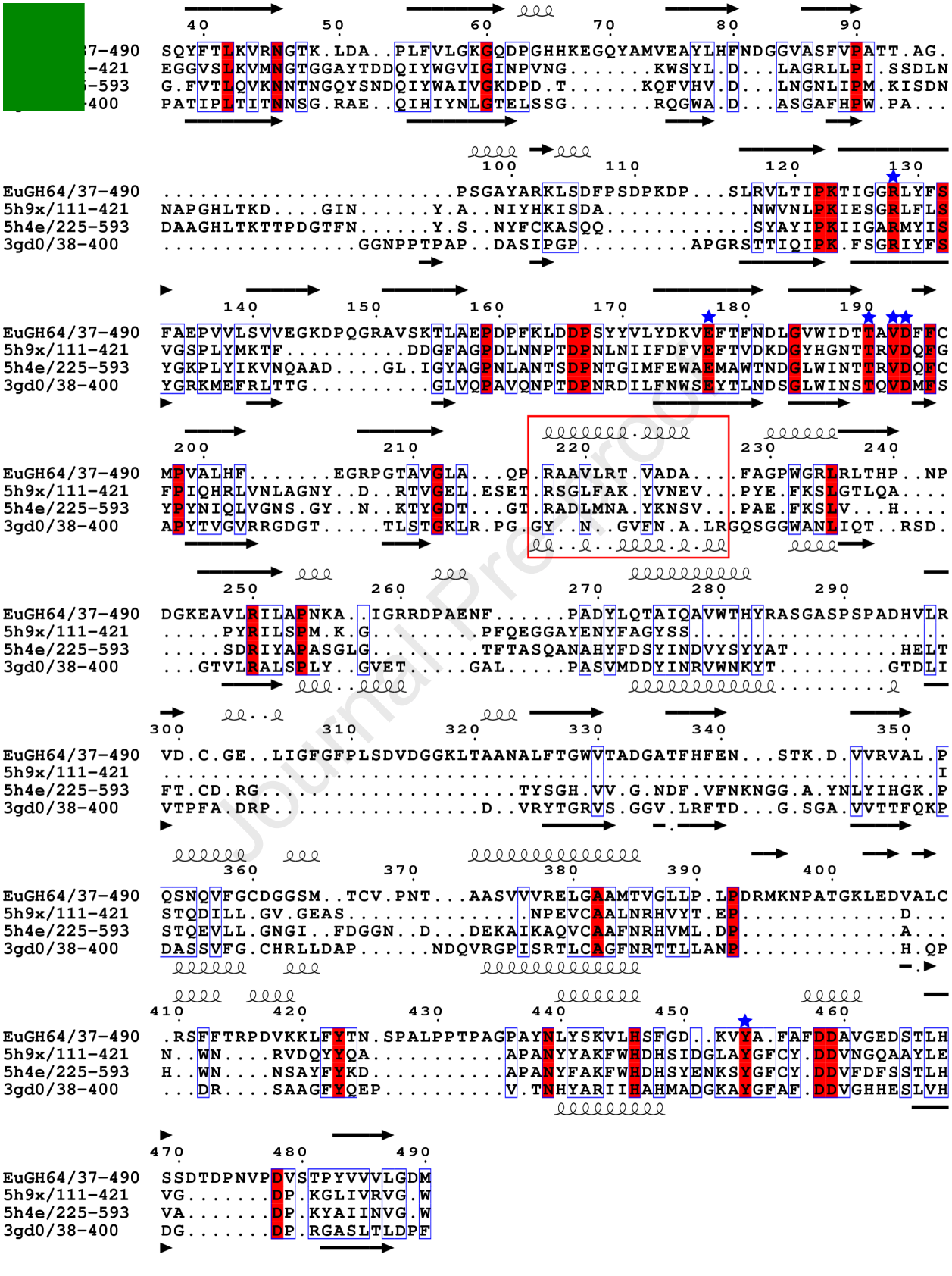

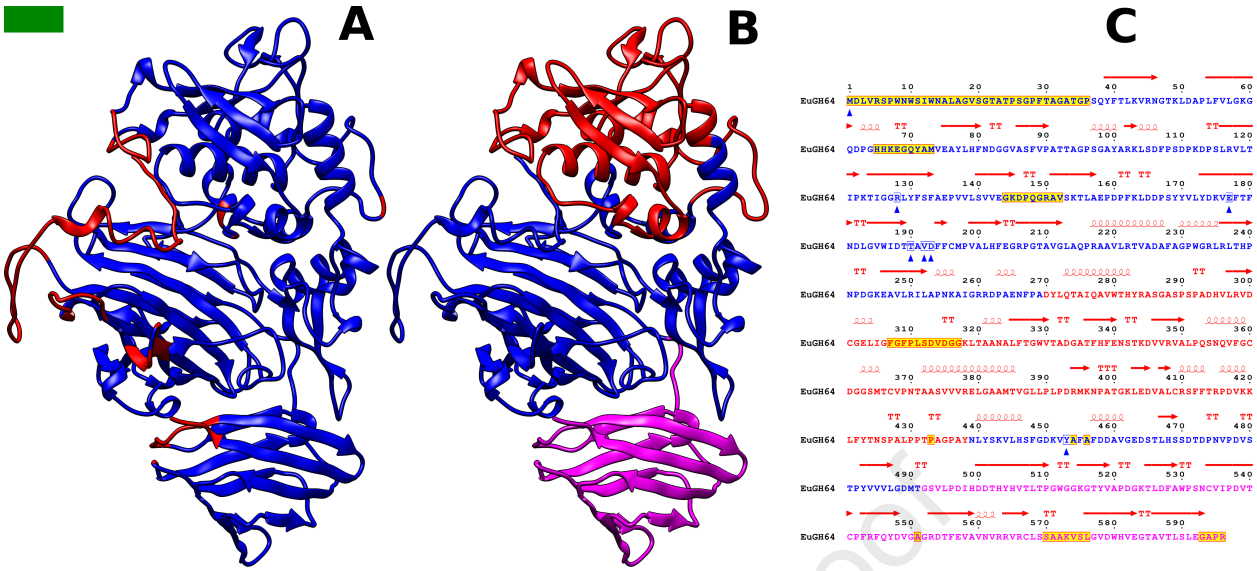

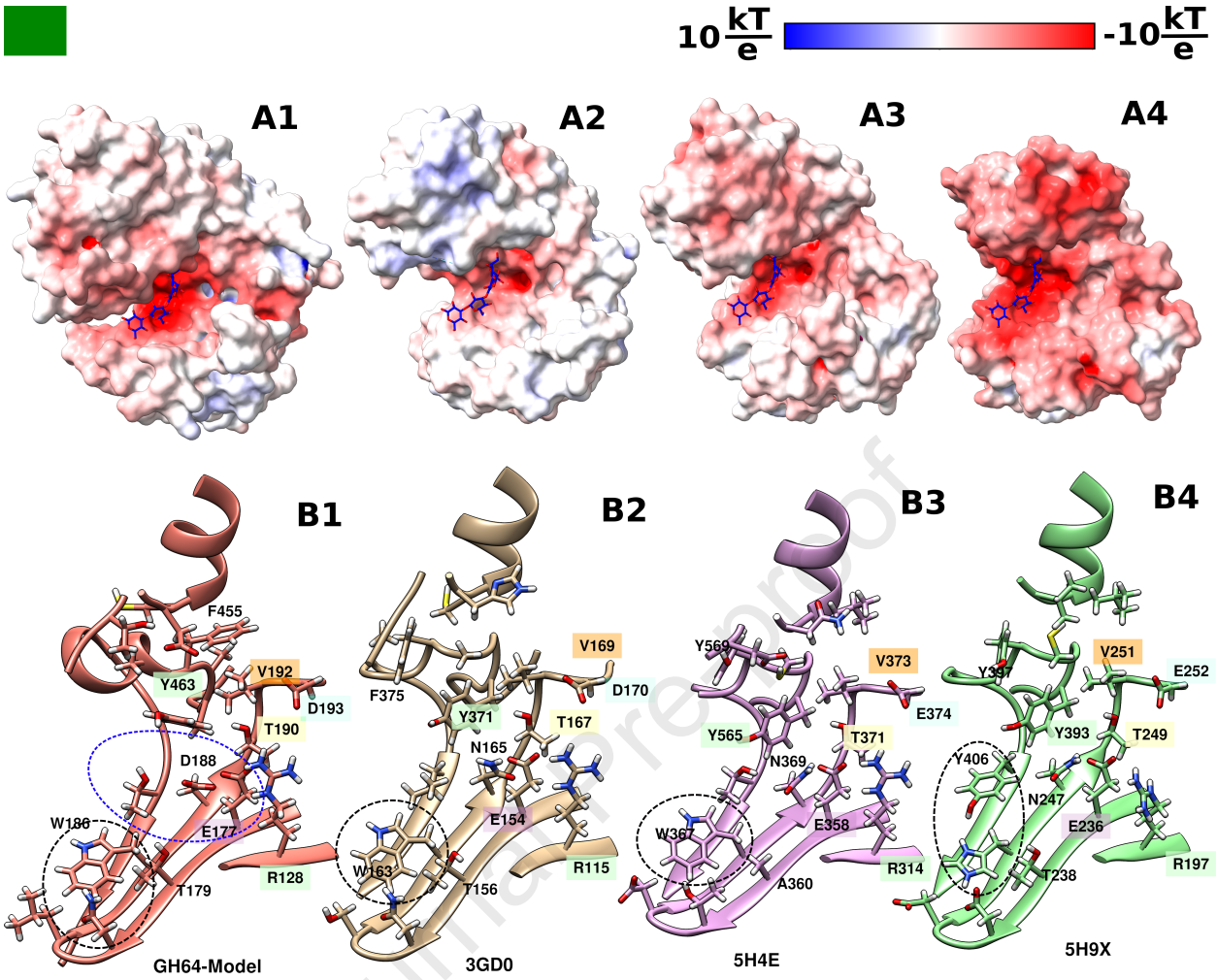

We identified a putative endo-β-1,3 glucanase (EgrGH64) in *Euglena gracilis*.

The gene was cloned and heterologously expressed in Escherichia coli.

EgrGH64 hydrolyzed paramylon, laminarin, and yeast cell wall

EgrGH64 probed to be a laminaripentaose-producing enzyme.

The purified enzyme inhibited yeast growth.

Conflict of Interest

The authors declare that they have no known competing financial interests or personal relationships that could have appeared to influence the work reported in this paper.